Stability of magnesium binary and ternary compounds for batteries determined from first principles

Mohsen Sotoudeh*,† and Axel Groß*,†

†*Institute of Theoretical Chemistry, Ulm University, Albert-Einstein-Allee 11, 89081 Ulm, Germany*

‡*Helmholtz Institute Ulm (HIU) for Electrochemical Energy Storage, Helmholtzstraße 11, 89069 Ulm, Germany*

E-mail: mohsen.sotoudeh@uni-ulm.de; axel.gross@uni-ulm.de

Abstract

Electrochemical stability is a critical performance parameter for the materials used as electrolytes and electrodes in batteries. Using first-principles electronic structure calculations, we have determined the electrochemical stability windows of magnesium binary and ternary spinel compounds. These materials are candidates for protective coating, solid electrolytes and cathodes in Mg-ion batteries, which represent a promising sustainable alternative to Li-ion batteries that still dominate the battery market. Furthermore, we have applied and assessed two different criteria for the chemical stability of compounds. For the spinel materials, we identify the critical role of the ionic radii of the transition metal for the stability of the compounds. In addition, we determine the ion mobility in these materials using a recently developed descriptor. We thus provide guidelines for the choice of promising solid materials for Mg-ion batteries with improved properties.

Keywords

stability window, density functional theory, magnesium batteries, magnesium binaries, ternary spinel chalcogenides, ion mobility

Introduction

Due to the importance of electrochemical energy storage devices for our future sustainable energy technology, there is a continuing quest for batteries with improved properties. In the last decades, lithium-ion batteries (LIBs) have dominated the battery market, but it appears that the increase of the performance of LIBs is now facing physico-chemical limits.[1] In order to overcome these limitations, either new advanced Li-ion technologies can be developed,[2] or alternative battery technologies that do not rely on Li, so-called post-Li-ion batteries,[3,4] can be employed. The post-Li-ion strategies switch to different mobile cations such as Na^+[4–7] or

Mg^{2+} [8–11] which might for example safely operate with a metal-anode leading to considerable improvements in energy densities[12,13] in a dendrite-free way.[14–18]

Among them, batteries based on the bivalent magnesium cation achieve higher volumetric energy densities compared to monovalent-based batteries.[12,13] However, this bivalent nature also leads to a stronger interaction with host lattices and solvents which limits the ionic conductivity.[19] Furthermore, decomposition of electrolytes on Mg electrodes,[20] forming passivation layers, reduces the battery performance. However, not only electrolytes, but also electrode materials can degrade when exposed to bivalent charge carriers. Hence the stability of battery materials is a critical parameter decisive for the performance and lifetime of batteries under operating conditions. This is for example reflected in the fact that in LIBs still in general flammable electrolytes are used, in spite of the hazards associated with such electrolytes,[18] simply due to the fact that there are still no effective and inexpensive alternative electrolytes available that are stable over the large potential range of more than 4 V required for LIBs.

In this computational study, we address the stability of magnesium binary and ternary compounds for batteries using first-principles periodic electronic structure calculations based on density functional theory. Mg binaries are simple compounds that can be used as coating materials for Mg metal anodes in order to prohibit elecrolyte degradation. In particular Mg halides have been identified as suitable coating materials due to a favorable electrochemical stability together with a suitable Mg ion mobility.[21,22] On the other hand, Mg ternary materials such as inorganic oxides,[23,24] hydrides,[25–27] and chalcogenides[28–30] exhibit good bulk Mg ionic conductivities. Among them, chalcogenide spinel lattices were identified as Mg-ion conductors with a high ion mobility[28,30] which is a critical property both for electrodes and solid electrolytes. Spinel compounds including transition metals such as Cr and Mn have high Mg binding energies[31] together with a satisfactory electron conductivity which makes them suitable as cathode materials. On the other hand, closed-shell systems such as Sc and Y have a rather low electron conductivity which is a prerequisite for their usage as solid

electrolytes.[28,32]

To be specific, we have determined the electrochemical stability window for a series of Mg binary and ternary compounds. Recently, we have developed a descriptor, the migration number, for the ion mobility that is based on the ionic radii, the oxidation states, and the difference in the Pauling electronegativities of the involved species.[33] These physical factors describe the height of the migration barriers of a series of binary, ternary and quaternary phases through linear scaling relation. Here we will particular focus on the fact whether the parameters entering the migration number are also decisive factors for the stability of the corresponding compounds. As far as the Mg-binaries are concerned, we will particularly focus on the electronegativity and link it to the band gaps of the considered materials.

With regard to the Mg ternaries, we concentrate on Mg sulfide spinels because of their favorable ion mobility properties.[28,32,33] We will vary the transition metals of these compounds and particular focus on the role of the ionic radius of the transition metal cation on the stability of the spinels. Again we will discuss the correlation between stability and ion mobility of these compounds. Thus we link two parameters that are critical for the performance of Mg-ion batteries and provide guidelines for the identification of promising alternative materials with improved properties.

Computational details

DFT calculations

First-principles calculations have been performed in the framework of density functional theory (DFT)[34,35] addressing the properties of binary Mg_nX_m and ternary MgB_2S_4 spinel compounds. The exchange-correlation effects were described by the generalized gradient approximation (GGA) functional PBE[36] and the hybrid functional HSE06[37] with a typical mixing factor of 0.2.

We have used the Vienna *Ab-initio* Simulation Package[38–40] together with projector aug-

mented wave (PAW)[40,41] method. The electronic structure was converged to 1×10^{-5} eV, applying a plane wave cutoff of 520 eV. A 4×4×4 k-point mesh has been used for the unit cells of the Mg_nX_m binaries. The ternary MgB_2S_4 spinel calculations were optimized using 2×2×2 k-point meshs for the unit cell containing eight formula units. The partial occupancies are set for each orbital using the tetrahedron method[42,43] and the so-called Blöchl corrections.[44] All atomic positions are optimized without symmetry constraints to obtain the ground state configurations. The initial configurations are taken from the Materials Project (MP) database.[45] We used the $Fd\bar{3}m$ space group for the MgB_2S_4 spinels, corresponding to a face-centered cubic structure. The Mg binaries ground state structures, as taken from the MP database, correspond to different space groups, as listed below.

In order to determine the Mg-ion migration barriers for the single-ion migration path between two tetrahedral sites passing the octahedral site, the nudged elastic band (NEB)[46,47] method has been applied in the low vacancy limit. In detail, we removed just one migrating cation within the supercell, for example resulting in a $Mg_{0.875}B_2S_4$ stoichiometry of the spinel compounds. In all binary and ternary compounds, a sufficiently large supercell has been chosen for the NEB calculations to ensure a negligible interaction between the periodic images of the migrating ions. All structures were fully relaxed until the forces on the atoms were converged within 0.05 eV $Å^{-1}$.

The NEB calculations have been carried out with seven distinct images for the binary compounds, and four distinct images for the ternary spinels to evaluate the Mg-ion migration minimum energy path. Note that the diffusion in the considered compounds corresponds to interstitial diffusion. The calcalutions for the ternary compounds were carried out in a charge-neutral fashion whereas for the binaries a compensating background charge was applied in the NEB calculations as in these materials typically the overall charge neutrality is ensured by an equal amount of anion and cation vacancies.

The stability window

The electrochemical stability window is commonly used to indicate the potential range in which the substance is neither oxidized nor reduced. Out of this range, the substance will react and decompose. We examine the implications of exposing the solid electrolytes to these high magnesium potentials without permitting any additional reaction between the electrolyte and the anode or cathode materials. The stability window is determined by the voltages at which magnesium is extracted from the electrolyte, forming an Mg-deficient decomposition layer between the solid electrolyte and the cathode, and when magnesium is inserted into the electrolyte, forming the Mg-reduced decomposition layer.

In the Mg binaries, below 0 V vs. Mg/Mg^{2+}, metallic Mg is the stable form. Above 0 V, the binaries consisting of oxidized Mg together with the anions are stable up to a voltage that corresponds to the formation energy ΔG_f^0, of the binaries,

$$\Delta V = -(\Delta G_f^0 / zF) \ , \tag{1}$$

where F is the Faraday constant and z corresponds to the elementary charges that are transferred upon the discharging reaction with $z = 2$ for Mg-ion batteries. At higher voltages, magnesium is extracted, providing the oxidized cations.

Ternary Mg-M-S phase diagrams are constructed for each spinel compounds utilizing a library of DFT computed bulk energies of materials with crystal structure from the Materials Project database ,[45] as shown in Fig. 1. The stability of ternary systems containing Mg, a second metal M, and sulfur will be briefly reviewed to demonstrate the principles and methodology involved. For the sake of simplicity, assume that only two binary sulfides of M, nominally MS and M_2S_3 (for Al, there is only Al_2S_3), are stable and no phases exist between Mg and M, and that only one ternary phase exists, MgM_2S_4. The thermodynamic parameters of the triangle MgM_2S_4-MgS-MS (for Al, $MgAl_2S_4$-MgS-Al) in Fig. 1 will determine its limits of stability in the low-potential magnesium-rich direction, and those in the triangle

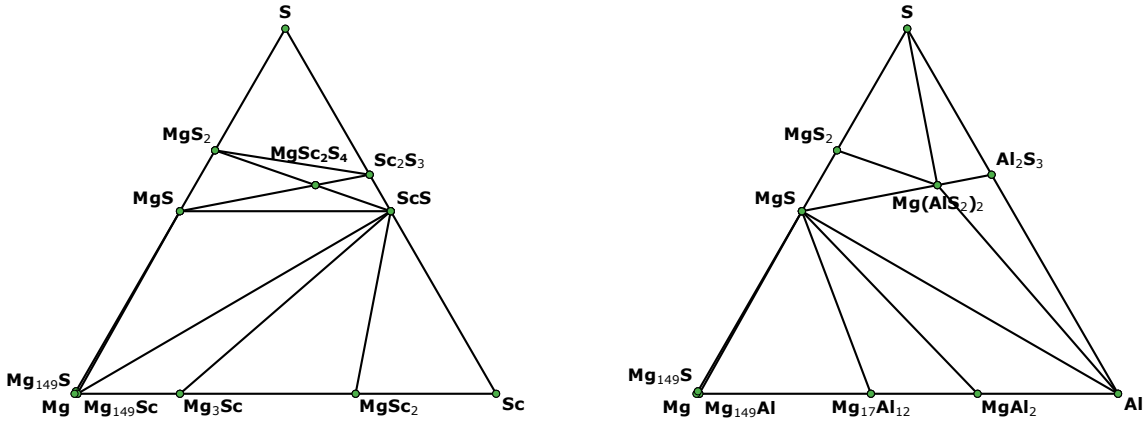

Figure 1: Ternary phase diagrams for the Mg–Sc–S and Mg–Al–S system. The labels and points correspond to the stable crystalline phases calculated by the energy above the hull. The lines underline the reaction vectors with respect to the different elemental concentrations for the stable phases.

MgM_2S_4-M_2S_3-MS (for Al, $MgAl_2S_4$-Al_2S_3-Al) will determine its limit of stability in the high-potential magnesium-poor direction, in the case of the possible solid electrolyte phase MgM_2S_4. Therefore, for these ternary spinels, the lower limit of the stability window has been obtained using the relevant Mg decomposition reaction between the solid electrolyte and the anode

$$\mathrm{Mg} + \mathrm{MgM_2S_4} \rightarrow 2\mathrm{MgS} + 2\mathrm{MS}, \tag{2}$$

$$3\mathrm{Mg} + \mathrm{MgAl_2S_4} \rightarrow 4\mathrm{MgS} + 2\mathrm{Al}, \tag{3}$$

and the minimum voltage vs. magnesium is determined from

$$V = -(\Delta G_r^0 / zF), \tag{4}$$

where

$$\Delta G_r^0 = \Delta G_f^0(products) - \Delta G_f^0(reactants). \tag{5}$$

Likewise, the maximum potential up to which this phase remains stable is determined by the Mg spinel decomposition reaction involving the solid electrolyte and the cathode

$$2\mathrm{MS} + \mathrm{MgM_2S_4} \rightarrow \mathrm{Mg} + 2\mathrm{M_2S_3}, \tag{6}$$

$$2\mathrm{Al} + 3\mathrm{MgAl_2S_4} \rightarrow 3\mathrm{Mg} + 4\mathrm{Al_2S_3}. \tag{7}$$

This can be converted to a voltage vs. magnesium by using Eqs. 4 and 5. Note that we determined the stabilities of all considered solid electrolytes for a temperature of 0 K.

Results and Discussion

Binary phases $\mathbf{Mg}_n\mathbf{X}_m$

The Mg binaries are the simplest ionic compounds that contain just the bivalent cation Mg^{2+} and one type of anion X^{n-} in various ratios depending in n. Different structures may exist for each composition depending on the relative sizes of the anions. We considered compositions with the commonly found stoichiometries in theoretical ground state configurations reported in the Materials Project (MP) database.[45] The local environment of the Mg-ion in the binary structures has been sketched in Fig. 2 for magnesium fluoride, oxide, bromide, and selenide together with the density of states (DOS) of the compounds. Whereas the PBE functional yields a good description of the minimum energy structurs and the relative energies of the Mg binaries, it typically underestimates the band gap of semiconductors and insulators.[47] Therefore the HSE06 hybrid functional has been used to get reliable band gaps. Note that a very low electron conductivity, typically reflected in a large band gap, is a prerequisite that a crystalline material can be used as a solid electrolyte,[1] but also as a protective coating.

The stable rutile structure of MgF_2 (Fig. 2a) reflects the strong tendency of Mg^{2+} to acquire an octahedral coordination. Each Mg atom is coordinated to six F atoms which connect to three Mg anions. The calculated HSE06 bandgap for MgF_2 of 10.37 eV is consistent

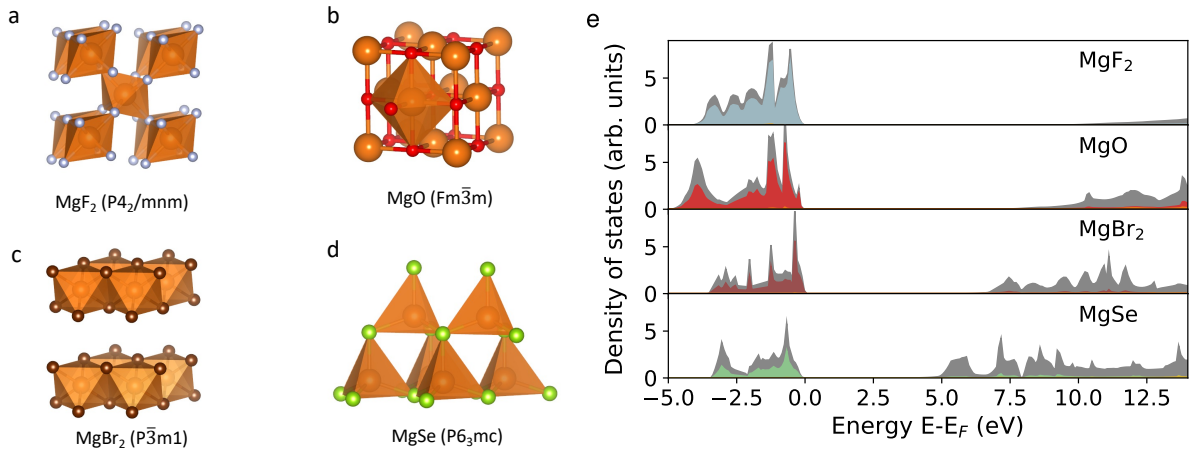

Figure 2: Structures of (a) MnF_2, (b) MgO, (c) $MgBr_2$, and (d) MgSe. Mg is colored orange, O red, F light blue, Br brown, and Se light green. The corresponding space groups of the binaries are provided in parentheses.The right graph (e) shows the calculated density of states (DOS) using the hybrid functional HSE06. The total DOS is given in black, and the projected DOS is shown in light blue for F-p, red for O-p, brown for Br-p, and light green for the Se-p orbitals, respectively

with the experimental value of 10.8 eV,[48] the largest for all Mg binary structures considered here. For this compound, the filled valence band is dominantly of F-p character (light blue) which extends from -4 to 0 eV. The rock-salt structure of MgO (Fig. 2b) is the structure in

Table 1: Space groups of the considered Mg binary compounds together with their band gaps in eV calculated with the HSE06 hybrid functional HSE06.

System	Space group	Band gap
MgH_2	$P4_2/mnm$	5.44
MgB_2	$P6/mmm$	0.00
Mg_2Si	$Fm\bar{3}m$	0.92
Mg_2Ge	$Fm\bar{3}m$	0.85
Mg_3N_2	$Ia\bar{3}$	3.01
Mg_3P_2	$Ia\bar{3}$	2.32
Mg_3As_2	$Ia\bar{3}$	2.14
MgO	$Fm\bar{3}m$	7.71
MgS	$Fm\bar{3}m$	4.26
MgSe	$P6_3mc$	4.67
MgTe	$P6_3mc$	3.92
MgF_2	$P4_2/mnm$	10.37
$MgCl_2$	$R\bar{3}m$	7.61
$MgBr_2$	$P\bar{3}m1$	6.44
MgI_2	$P\bar{3}m1$	4.79

which the cations occupy all octahedral sites in a cubic close packed array of anions. Both anions and cations are six-fold coordinatated, an octahedron of six counter-ions surrounds each ion. The calculated bandgap of 7.71 eV is in good agreement with the experimental result of 7.77 eV.[49] The filled valence band of MgO is of dominantly O-p character (red), extending from -5 to 0 eV. The $MgBr_2$ compound (Fig. 2c) shows a layered structure in which the close-packed layers are bonded via weak van der Waals interactions between the bromine atoms of the adjacent layers. Each Mg cation is surrounded by six Br anion. The calculated bandgap of this compound is 6.44 eV. The filled valence band of $MgBr_2$ consists mainly of Br-p states (brown) extending from -3.5 to 0 eV. In the wurtzite structure of MgSe (Fig. 2d), the Mg cations occupy half the tetrahedral sites. In this structure, both cations and anions are fourfold coordinated. The local symmetries of the cations and anions are identical with respect to their nearest neighbors but differ at the second-nearest neighbor distances. This compound exhibits a bandgap of 4.67 eV. Like other Mg binary compounds, the valence band is dominated by p orbitals (light green) of the anion.

The band gaps of all considered Mg binaries calculated with the HSE functional together with their ground state space group are listed in Tab 1. Magnesium diboride MgB2 has no bandgap, whereas magnesium silicide (Mg_2Si) and germanide (Mg_2Ge) exhibit small bandgaps below 1 eV. The remaining compounds show a broad range of band gaps of up to 10.37 eV for MgF_2. Most of them have band gaps higher than 3 eV which effectively make them to insulators whereas magnesium phosphide (Mg_3P_2) and arsenide (Mg_3As_2) have band gaps slightly above 2 eV.

In order to understand the origin of the wide range of band gaps observed in the Mg binaries, we have plotted the band gaps as a function of the Pauling electronegativity of the Mg binding partners in the binaries in Fig. 3a. We find a strong correlation between electronegativity and band gaps, reflected in an approximate linear scaling between these two properties. Strongly electronegative anions such as F indicative of strong ionic bonding characteristics lead to a wide bandgap, whereas weakly electronegative anions such as B with

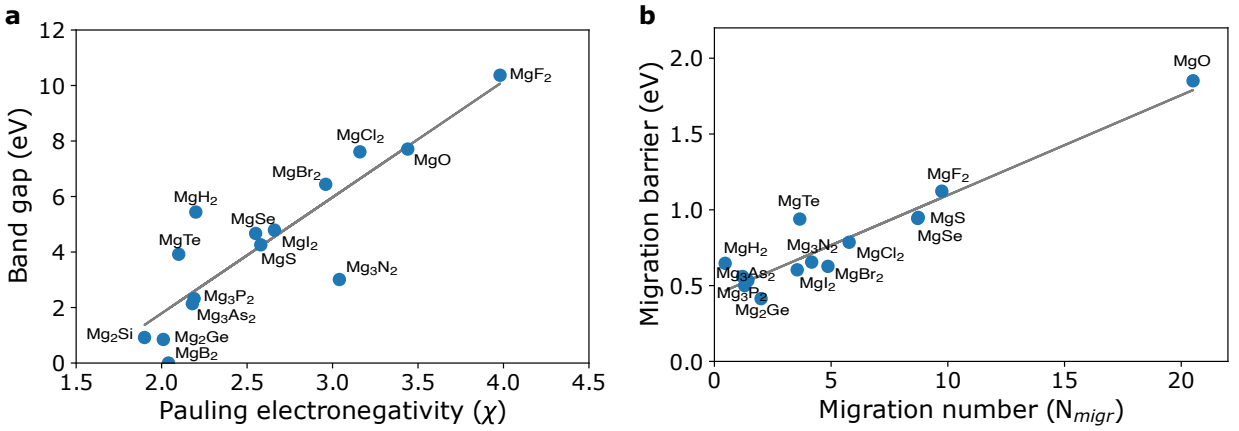

Figure 3: Electronegativity effects on the band gaps and migration barriers of Mg binaries. (a) The calculated band gap of Mg binaries using the hybrid functional HSE06 as a function of the anion electronegativity (χ). The grey line is a linear regression of these results. (b) The migration barriers of Mg binaries, derived from periodic DFT-PBE calculations combined with the NEB method, as a function of the migration number (N_{migr}).

metallic bonding characteristics show small or vanishing band gaps.

The electrochemical stability windows of the binary compounds vs. Mg/Mg^{2+} calculated according to Eq. 1 are plotted in Fig. 4. For binaries, Mg-triels and Mg-tetrels exhibit poor stability reflected in the small stability window and consequently low oxidation resistance. Mg-pnictogens are associated with a larger stability window. For example, the Mg_3N_2 will be stable over a range from 0 to 0.75 V at room temperature. However, the widths of the stability windows are still rather small (<1.0 V). In contrast, all of the Mg-halogens and Mg-chalcogens are notably more stable over a broader range of potentials at room temperature. Interestingly, the oxidative stabilities exhibit a strong correlation with the anion electronegativities. For a strongly electronegative anion such as F, the corresponding binary MgF_2 compound is stable against Mg up to potentials of more than 5 V. Consequently, among all considered binaries, Mg chalcogenides and halides exhibit the highest stability.

A further critical parameter for solid-state electrolytes is their ionic conductivity. From a crystallographic perspective, ionic crystals such as Mg binaries are characterized by two sublattices, namely a cationic sublattice and an anionic sublattice. Typically, the diffusion of ions is restricted to their corresponding sublattice. Thus, Mg^{2+} diffusion mechanism is re-

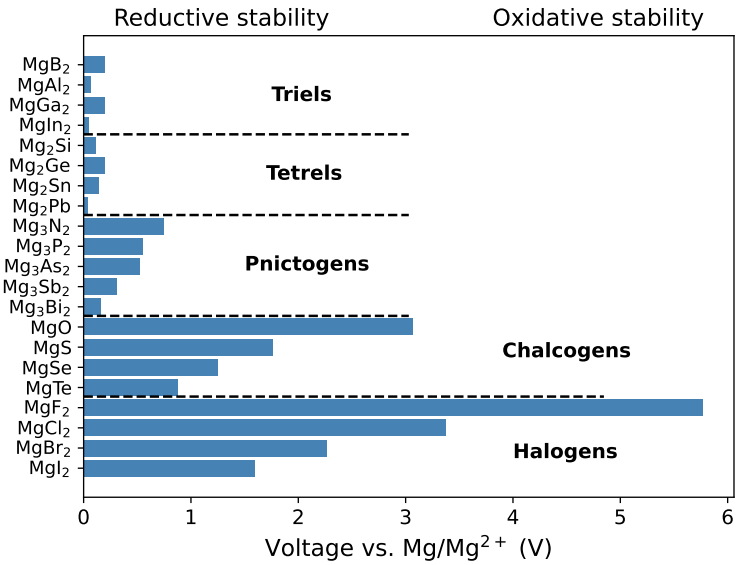

Figure 4: Electrochemical stability windows of Mg binaries indicating the voltages vs. Mg metal that the binaries are stable and not decomposed. Compounds are listed through the anions group in the periodic table.

stricted to the cationic sublattices, diffusion mechanisms correlated with the anion sublattice (interstitialcy) do usually not occur. In such ionic crystals, diffusion and ionic conduction requires the presence mobile point defects. Note that usually the defect concentration is small in the pure ionic crystals, even close to the melting temperature. For example, ionic crystals such as MgO or NaCl show low ionic conductivities even at high temperatures, caused by the small point defect concentration.

In alkali halides, Schottky disorder in which both cation vacancies (VC) and anion vacancies (VA) create vacancy defect pairs, is dominant. In undoped crystals with Schottky disorder, equal site fractions of cation and anion vacancies are required for charge neutrality reasons. In thermal equilibrium, the product of the vacancy concentrations for the cations, C_{V_C}, and of the anions, C_{V_A}, is temperature-depending according to

$$C_{V_C} C_{V_A} = \exp\left(-\frac{G_{SP}}{k_{\mathrm{B}} T}\right) = K_{SP}(T) \tag{8}$$

where G_{SP} is the Gibbs free energy for the Schottky pair formation, $K_{SP}(T)$ denotes the

Schottky product. In order to ensure an equal amount of anion and cation vacancies in our migration barrier simulations, a compensating background charge was applied in the NEB calculations for the binary compounds using the PBE functional.

Recently, we proposed a descriptor for the ion mobility, the so-called migration number:[33]

$$N_{migr} = (r_{\mathrm{Mg}} + r_{\mathrm{X}}) n_{\mathrm{Mg}} n_{\mathrm{X}} \Delta\chi^2 / (N_{\mathrm{Mg}} + N_{\mathrm{X}}) \ , \tag{9}$$

where r_i and n_i are the ionic radius of species i and its oxidation state, $\Delta\chi^2$ is the square of the difference in the electronegativities between migrating cations and the counter anions of the lattice, and N_i is the number of atoms of the corresponding species in the unit cell of the crystal. For all considered Mg binary materials, the calculated migration barriers as a function of migration number (N_{migr})[33] are plotted in Fig. 3b. The square of the electronegativity difference quantifies the role of the deviation from a purely ionic interaction between migrating cation and the anions of the host lattice which contribute to the bonding in a nominally ionic crystal.[32,33] We find a linear scaling between the migration number and the calculated migration barrier, giving the descriptor a predictive power with respect to the migration barriers of new binary compounds.[33] For the outliers from the linear scaling relation in Fig. 3b, additional factors play a role such as the Pauli repulsion.[50]

According to the calculations and an analysis of the migration number, MgF_2 and MgO are associated with high Mg migration barriers of above 1 eV which is related to strong ionic bonding characteristics reflected in the large difference in the electronegativity. In contrast, Mg_2Ge with metallic bonding characteristics indicated by the small electronegativity difference exhibits a very low migration barrier (less than 0.5 eV). The remaining Mg-halides, Mg-chalcogenides, Mg-pnictides, and Mg-tetrels have intermdiate bonding characteristics between ionic and metallic bonding. MgS and MgSe, with an electronegativity difference of about 1.3, exhibit a barrier of 0.9 eV. Mg migration in $MgCl_2$, $MgBr_2$, and Mg_3N_2 with an electronegativity difference of 1.7 is hindered by a barrier of about 0.7 eV. Combining the

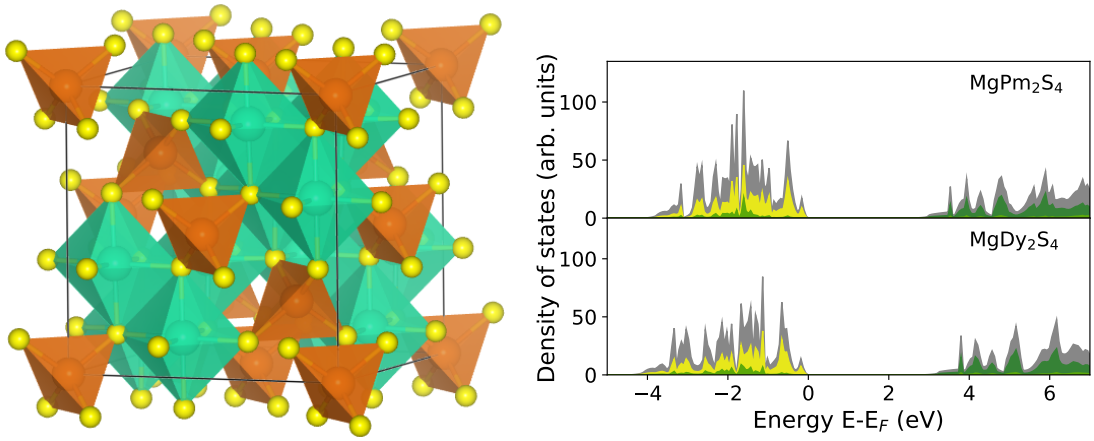

Figure 5: Structure of MgB_2S_4 spinel. The Mg atoms (orange) occupy the tetrahedral sites, while the B species (spring green) only occupy octahedral sites. The yellow spheres denote the S^{2-} anions. The right graph shows the calculated density of states (DOS) using the HSE06 hybrid functional for $MgPm_2S_4$ and $MgDy_2S_4$ compounds. The total DOS is given in gray, and the projected DOS are shown in yellow for S-*p* orbitals, and green for both Tm-*d* and Dy-*d* states.

results of the stability analysis shown in Fig. 4 with the results for the ion mobility shown in Fig. 3b, among all considered binaries the halides $MgCl_2$, $MgBr_2$, and MgI_2 represent a compromise between a large electrochemical stability window with a sufficiently small migration barrier, making them promising candidates for coating materials in Mg batteries.

Ternary phases MgB_2S_4

Passing from Mg binaries to Mg ternary spinels with the general formula of MgB_2S_4, the compositional complexity increases to three different species. The spinel structure consists of a cubic close packed array of S^{2-} anions in which the Mg cations occupy one-eighth of the tetrahedral holes, and the B cations occupy half the octahedral holes (Fig. 5). Structurally, a large numbers of vacant sites is available, and the open crystal structure in principle allows a migrating atom to move rather freely through the lattice.

Recently, the spinel framework was proposed as a potential candidate for solid electrolytes of multivalent ion batteries such as Mg due to the rather low activation energy for migration, E_a.[28,30,32] On the atomic scale, the migration pathway of Mg^{2+} in a sulfide spinel structure

starts from the energetically most favorable tetrahedral site and proceeds to the next nearest neighboring tetrahedral site by passing the metastable octahedral site in a straight line. The stability of the Mg-ion in the tetrahedral site is lower than predicted from a pure electrostatic model due to the strong covalent nature of the Mg-S interaction.[32]

We have addressed lanthanoid and empty *d*-shell sulfide spinels to find appropriate Mg conductors that balance stability and high ion mobility. Electronically, in this particular transition metal spinels the *d*-band occupancy is zero, resulting in a large bandgap between the filled valence band, which is dominated by sulfur *p* orbitals indicated in yellow in Fig. 5, and the empty *d*-band (green) as the conduction band.

We have evaluated the electronic structure of all MgB_2S_4 spinel compounds employing the HSE06 hybrid functional. $MgCe_2S_4$, $MgEu_2S_4$, and $MgYb_2S_4$ represent no electronic bandgap, while other spinel compounds can be classified into the mid-range bandgap materials (more than 2.5 eV), possessing a rather poor electronic conductivity and can thus be regarded as insulating materials. Therefore, the first criterion necessary for the use as SSEs or coatings is satisfied in these structures.

The next step in proposing suitable and practical materials for the electrolyte phase is the assessment of stability limits in the low-potential magnesium-rich and high-potential magnesium-poor directions. For this purpose, the electrolyte stability windows of the considered ternary spinel phases have been determined using the Gibbs free energy of the phases according to Eq. 4 and 5, as shown in Fig. 6. The reductive stability reactions are determined by the triangle MgM_2O_4-MgS-MS, whereas the oxidative stability is calculated using the metal sulfide phases MgM_2O_4-M_2S_3-MS. According to Fig. 6, all calculated stability windows are smaller than 1.8 V. Among the considered candidates, those sulfide spinels with large ionic radii of the B-cation (La, Ce, Pr, Nd, Pm, and Sm) display narrow stability windows due to the instability against Mg metal. The largest stability windows are found for the metals Lu, Y, and Sc.

Note that also the ionic radii r_i of the constituents have been used[51] to predict the stability

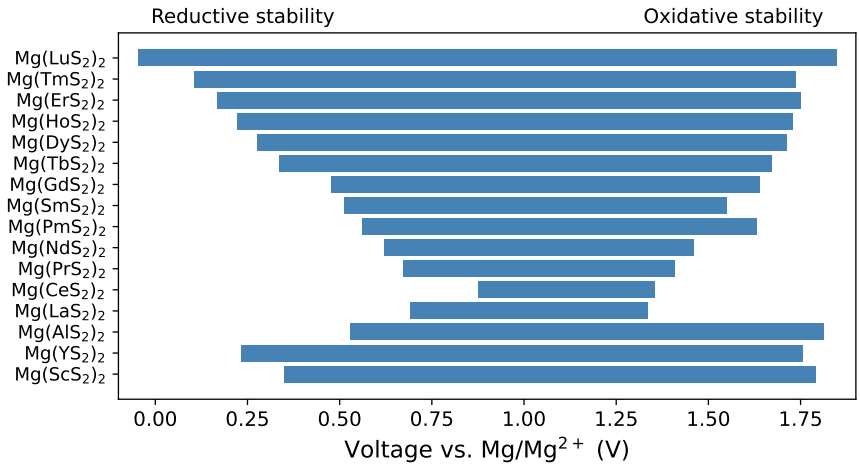

Figure 6: Electrochemical stability windows of the considered MgB_2S_4 compounds as a funtion of the voltages vs. Mg metal.

of spinel compounds based on the so-called the tolerance factor, τ which is a dimensionless number based on the ratio of the sum of ionic radii of all ions (A, B, X):

$$\tau = \frac{\sqrt{3}(r_B + r_X)}{2(r_A + r_X)} \ . \tag{10}$$

The tolerance factor is derived from the geometrical relationship between the different polyhedra being present in some materials including perovskites and garnets. A tolerance factor of less than one reflects the presence of compressed octahedra which is associated with the fact that the normal spinel structure becomes the most stable configuration. Table 2 collects, among other properties, the calculated tolerance factors τ of the spinel materials considered in this study. All values are within the range $0.8 < \tau < 1$, indicating that all compounds should be stable as spinels and thus producible.

In order to check the reliability of structure prediction according to the tolerance factor, a more accurate estimate of the stability of these spinel structures relative to competing polymorphs and competing compounds was investigated using the energy above the convex hull of stable compounds in each chemical space, E_{hull}. Stable compounds have E_{hull}=0, and synthesizability of sulfides has been observed up to E_{hull}=0.05 eV/atom.[52] In Fig. 7a, the

Table 2: The calculated migration barriers (eV), tolerance factors (τ), and B-cation ionic radii r_B (given in pm) of MgB_2S_4 normal spinel structure.

Compound	r_B (pm)	Migration barrier (eV)	Tolerance factor (τ)
$MgAl_2S_4$	67.5	0.484	0.803
$MgSc_2S_4$	88.5	0.415	0.874
MgY_2S_4	104.0	0.360	0.927
$MgLa_2S_4$	117.2	0.478	0.972
$MgPr_2S_4$	113.0	0.429	0.957
$MgNd_2S_4$	112.3	0.398	0.955
$MgPm_2S_4$	111.0	0.368	0.951
$MgSm_2S_4$	109.8	0.357	0.947
$MgGd_2S_4$	107.8	0.354	0.940
$MgTb_2S_4$	106.3	0.353	0.935
$MgDy_2S_4$	105.2	0.358	0.931
$MgHo_2S_4$	104.1	0.365	0.927
$MgEr_2S_4$	103.0	0.379	0.924
$MgTm_2S_4$	102.0	0.386	0.920
$MgLu_2S_4$	100.1	0.407	0.914

energies above the convex hull for all compounds considered in this structure are plotted as a function of the ionic radius of the B cation. First of all It should be noted that the unit-cell volume of the spinel structure increases by substituting a larger B cation. For ionic radii of the B cation above about 110 pm, the energy above the convex hull in general becomes larger than 0.05 eV/atom. This indicates that larger ionic radii lead to a destabilization of the spinel structure and thus to a preference for non-spinel-type structures.

The different stability indicators can be assessed as follows: The tolerance factor τ gives a rough crystallographically-based estimate for the stability of the spinel compounds using only ionic radii. The energy above the convex hull E_{hull} additionally yields the stability with respect to competing compound structures and polymorphs. Still, the electrochemical stability window appears to be the crucial quantity with respect to the stability of these materials as solid electrolytes and coating materials.

In order to additionally provide a general idea about the chemical trends in the migration energy barrier with respect to the size of the transition metals used in the spinel materials, in Fig. 7b also the migration energy is plotted as a function of the B-cation ionic radii.

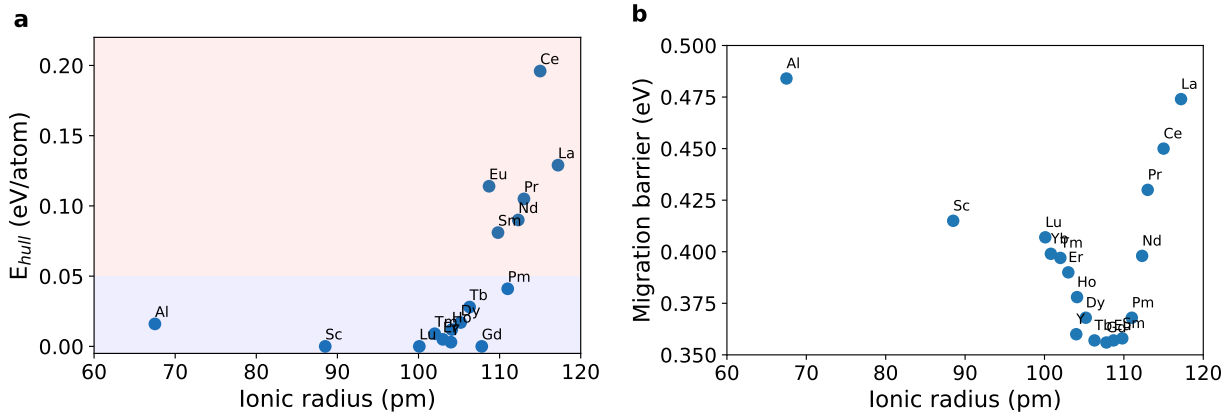

Figure 7: Dependence of the energies above the convex hull, E_{hull} and the migration barriers as a function of the ionic radii of the B cation in sulfide spinels. (a) Energy above the convex hull E_{hull} in eV.The blue region represents the range of stable sulfide spinels whereas the red area corresponds to unstable compounds. (b) Calculated migration barriers (in eV).

The NEB method was applied to determine the migration barrier. A strong correlation between the B-cation ionic radius and the calculated migration barriers is observed with a pronounced minimum for radii between 100 to 110 pm, indicating a high Mg-ion mobility in this range. Thus the choice of the transition metal B allows to tune the ion mobility in the spinel compounds.

Next we consider the details of the Mg migration in more detail. In Fig. 8, the energy profiles along the Mg migration path from the tetrahedral site across the octahedral site to the next tetrahedral site are shown. The tetrahedral site is the energetically most stable site for Mg in all considered compounds. The octahedral site corresponds to a local minimum for all compounds except for $MgLa_2S_4$, $MgPr_2S_4$, $MgNd_2S_4$, and $MgPm_2S_4$. Although increasing the B-cation size in sulfide spinels first leads to a decrease in the Mg^{2+} migration barrier, for radii larger than 1.1 Å such as Pm, Nd, Pr, Ce, and La the transition state energy rises again, as illustrated in Fig. 7b, as a consequence of the fact that the octahedral site becomes energetically more costly,[53] finally even making the octahedral site to the transition state for migration. Interestingly, those compounds in which the octahedral site becomes the transition state are unstable.

This correlation indicates that the size of the B cations plays a dominant role with

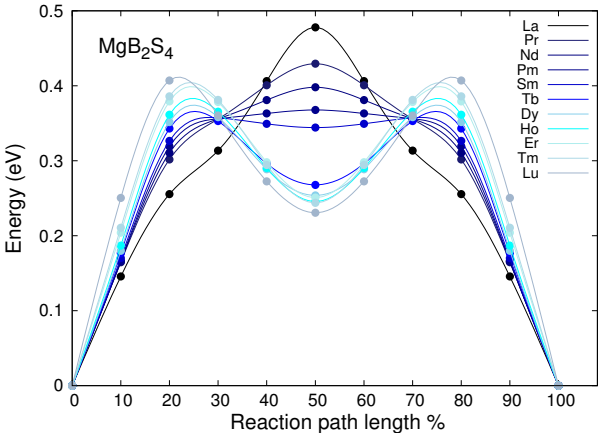

Figure 8: The Mg^{2+} migration energy barriers (in eV) as a function of the reaction path coordinate derived from periodic DFT calculations combined with NEB for the single-ion migration between two tetrahedral sites across the octahedral site. The calculations are performed in the high-concentration limit namely with a $Mg_{0.875}B_2S_4$ stoichiometry.

respect to the height of the Mg-ion migration barriers as well as for the stability of the spinel compounds. The B-cation ionic radius is decisive for the equilibrium B-S bond length and thus also influences the strength of this bond. Qualitatively, enlarging the bonds should lower their bonding strength which reduces the stability of the spinel compounds.

Note that in spite of the variation in the height of the Mg migration barriers in the MgB_2S_4 spinels, the calculated barrier heights are all in the range between 0.35 and 0.49 eV which makes them good ionic conductors.[54] Furthermore, those of the compounds with B-cation radii smaller than 1.1 Å are also chemically stable so that one should be able to prepare these compounds. Still, all of them have electrochemical stability windows that are below 1.8 V, with the Lu, Y, and Sc spinel compounds having the largest electrochemical stability window.

Conclusions and Summary

In summary, the electrochemical stability windows of Mg binary and spinel sulfide compounds together with their Mg migration paths have been computed using DFT calculations in order to assess their feasibility as solid electrolytes or potential coating materials. Among

the considered binaries, $MgBr_2$, MgI_2, and $MgCl_2$ exhibit a good stability against the highly reductive Mg metal anode as well as an acceptable Mg^{2+} mobility. Furthermore, our study highlights the critical role of the Pauling electronegativity for the band gap and the ionic conductivity of these binary compounds. For the sulfide spinel compounds, the B-cation ionic radius has been identified to play a dominant role with respect to the stability and Mg migration energy barriers. All considered compounds exhibit sufficiently low Mg migration barrier, but only $MgLu_2S_4$, MgY_2S_4, and $MgSc_2S_4$ have been found to be electrochemically stable over a voltage range close to 2 V. We trust that these insights will serve as valuable design guidelines for developing fast Mg conducting solid materials with improved properties.

Acknowledgements

This work contributes to the research performed at CELEST (Center for Electrochemical Energy Storage Ulm-Karlsruhe) and was funded by the German Research Foundation (DFG) under Project ID 390874152 (POLiS Cluster of Excellence). Further support by the Dr. Barbara Mez-Starck Foundation and computer time provided by the state of Baden-Württemberg through bwHPC and the German Research Foundation (DFG) through grant no INST 40/575-1 FUGG (JUSTUS 2 cluster) are gratefully acknowledged.

References

(1) Janek, J.; Zeier, W. G. A solid future for battery development. *Nat. Energy* **2016**, *1*, 16141.

(2) Choi, S.; Wang, G. Advanced Lithium-Ion Batteries for Practical Applications: Technology, Development, and Future Perspectives. *Adv. Mater. Technol.* **2018**, *3*, 1700376.

(3) Elia, G. A.; Marquardt, K.; Hoeppner, K.; Fantini, S.; Lin, R.; Knipping, E.; Pe-

ters, W.; Drillet, J.-F.; Passerini, S.; Hahn, R. An Overview and Future Perspectives of Aluminum Batteries. *Adv. Mater.* **2016**, *28*, 7564–7579.

(4) Anji Reddy, M.; Helen, M.; Groß, A.; Fichtner, M.; Euchner, H. Insight into Sodium Insertion and the Storage Mechanism in Hard Carbon. *ACS Energy Lett.* **2018**, *3*, 2851–2857.

(5) Hwang, J.-Y.; Myung, S.-T.; Sun, Y.-K. Sodium-ion batteries: present and future. *Chem. Soc. Rev.* **2017**, *46*, 3529–3614.

(6) Yabuuchi, N.; Kubota, K.; Dahbi, M.; Komaba, S. Research Development on Sodium-Ion Batteries. *Chem. Rev.* **2014**, *114*, 11636–11682.

(7) Euchner, H.; Vinayan, B. P.; Reddy, M. A.; Fichtner, M.; Groß, A. Alkali metal insertion into hard carbon – the full picture. *J. Mater. Chem. A* **2020**, *8*, 14205–14213.

(8) Gregory, T. D.; Hoffman, R. J.; Winterton, R. C. Nonaqueous Electrochemistry of Magnesium: Applications to Energy Storage. *J. Electrochem. Soc.* **1990**, *137*, 775–780.

(9) Aurbach, D.; Lu, Z.; Schechter, A.; Gofer, Y.; Gizbar, H.; Turgeman, R.; Cohen, Y.; Moshkovich, M.; Levi, E. Prototype systems for rechargeable magnesium batteries. *Nature* **2000**, *407*, 724–727.

(10) MacLaughlin, C. M. Status and Outlook for Magnesium Battery Technologies: A Conversation with Stan Whittingham and Sarbajit Banerjee. *ACS Energy Lett.* **2019**, *4*, 572–575.

(11) Davidson, R.; Verma, A.; Santos, D.; Hao, F.; Fincher, C. D.; Zhao, D.; Attari, V.; Schofield, P.; Van Buskirk, J.; Fraticelli-Cartagena, A. et al. Mapping mechanisms and growth regimes of magnesium electrodeposition at high current densities. *Mater. Horiz.* **2020**, *7*, 843–854.

(12) Singh, N.; Arthur, T. S.; Ling, C.; Matsui, M.; Mizuno, F. A high energy-density tin anode for rechargeable magnesium-ion batteries. *Chem. Commun.* **2013**, *49*, 149–151.

(13) Zhao-Karger, Z.; Gil Bardaji, M. E.; Fuhr, O.; Fichtner, M. A new class of non-corrosive, highly efficient electrolytes for rechargeable magnesium batteries. *J. Mater. Chem. A* **2017**, *5*, 10815–10820.

(14) Aurbach, D.; Cohen, Y.; Moshkovich, M. The Study of Reversible Magnesium Deposition by In Situ Scanning Tunneling Microscopy. *Electrochem. Solid-State Lett.* **2001**, *4*, A113.

(15) Matsui, M. Study on electrochemically deposited Mg metal. *J. Power Sources* **2011**, *196*, 7048 – 7055.

(16) Zhao, Q. S.; Wang, J. L. Reversibility of electrochemical magnesium deposition from tetrahydrofuran solutions containing pyrrolidinyl magnesium halide. *Electrochim. Acta* **2011**, *56*, 6530.

(17) Jäckle, M.; Groß, A. Microscopic properties of lithium, sodium, and magnesium battery anode materials related to possible dendrite growth. *J. Chem. Phys.* **2014**, *141*, 174710.

(18) Jäckle, M.; Helmbrecht, K.; Smits, M.; Stottmeister, D.; Groß, A. Self-diffusion barriers: Possible descriptors for dendrite growth in batteries? *Energy Environ. Sci.* **2018**, *11*, 3400–3407.

(19) Huie, M. M.; Bock, D. C.; Takeuchi, E. S.; Marschilok, A. C.; Takeuchi, K. J. Cathode materials for magnesium and magnesium-ion based batteries. *Coord. Chem. Rev.* **2015**, *287*, 15 – 27.

(20) Buchner, F.; Forster-Tonigold, K.; Bolter, T.; Rampf, A.; Klein, J.; Groß, A.; Behm, R. J. Interaction of Mg with the ionic liquid 1-butyl-1-methylpyrrolidinium bis(trifluoromethylsulfonyl)imide – An experimental and computational model study

of the electrode–electrolyte interface in post-lithium batteries. *J. Vac. Sci. Technol. A* **2022**, *40*, 023204.

(21) Chen, T.; Ceder, G.; Sai Gautam, G.; Canepa, P. Evaluation of Mg Compounds as Coating Materials in Mg Batteries. *Front. Chem.* **2019**, *7*, 24.

(22) Chen, T.; Sai Gautam, G.; Canepa, P. Ionic Transport in Potential Coating Materials for Mg Batteries. *Chem. Mater.* **2019**, *31*, 8087–8099.

(23) Ikeda, S.; Takahashi, M.; Ishikawa, J.; Ito, K. Solid electrolytes with multivalent cation conduction. 1. Conducting species in Mg-Zr-PO_4 system. *Solid State Ionics* **1987**, *23*, 125 – 129.

(24) Halim, Z.; Adnan, S.; Mohamed, N. Effect of sintering temperature on the structural, electrical and electrochemical properties of novel $Mg_{0.5}Si_2(PO_4)_3$ ceramic electrolytes. *Ceram. Int.* **2016**, *42*, 4452 – 4461.

(25) Mohtadi, R.; Matsui, M.; Arthur, T. S.; Hwang, S.-J. Magnesium Borohydride: From Hydrogen Storage to Magnesium Battery. *Angew. Chem. Int. Ed.* **2012**, *51*, 9780–9783.

(26) Unemoto, A.; Matsuo, M.; Orimo, S.-i. Complex Hydrides for Electrochemical Energy Storage. *Adv. Funct. Mater.* **2014**, *24*, 2267–2279.

(27) Higashi, S.; Miwa, K.; Aoki, M.; Takechi, K. A novel inorganic solid state ion conductor for rechargeable Mg batteries. *Chem. Commun.* **2014**, *50*, 1320–1322.

(28) Canepa, P.; Bo, S.-H.; Sai Gautam, G.; Key, B.; Richards, W. D.; Shi, T.; Tian, Y.; Wang, Y.; Li, J.; Ceder, G. High magnesium mobility in ternary spinel chalcogenides. *Nat. Commun.* **2017**, *8*, 1759.

(29) Koettgen, J.; Bartel, C. J.; Ceder, G. Computational investigation of chalcogenide spinel conductors for all-solid-state Mg batteries. *Chem. Commun.* **2020**, *56*, 1952–1955.

(30) Dillenz, M.; Sotoudeh, M.; Euchner, H.; Groß, A. Screening of Charge Carrier Migration in the $MgSc_2Se_4$ Spinel Structure. *Front. Energy Res.* **2020**, *8*, 260.

(31) Liu, M.; Rong, Z.; Malik, R.; Canepa, P.; Jain, A.; Ceder, G.; Persson, K. A. Spinel compounds as multivalent battery cathodes: a systematic evaluation based on ab initio calculations. *Energy Environ. Sci.* **2015**, *8*, 964–974.

(32) Sotoudeh, M.; Dillenz, M.; Groß, A. Mechanism of Magnesium Transport in Spinel Chalcogenides. *Adv. Energy Sustainability Res.* **2021**, *2*, 2100113.

(33) Sotoudeh, M.; Groß, A. Descriptor and Scaling Relations for Ion Mobility in Crystalline Solids. *JACS Au* **2022**, *2*, 463–471.

(34) Hohenberg, P.; Kohn, W. Inhomogeneous Electron Gas. *Phys. Rev.* **1964**, *136*, B864–B871.

(35) Kohn, W.; Sham, L. J. Self-Consistent Equations Including Exchange and Correlation Effects. *Phys. Rev.* **1965**, *140*, A1133–A1138.

(36) Perdew, J. P.; Burke, K.; Ernzerhof, M. Generalized Gradient Approximation Made Simple. *Phys. Rev. Lett.* **1996**, *77*, 3865–3868.

(37) Heyd, J.; Scuseria, G. E.; Ernzerhof, M. Hybrid functionals based on a screened Coulomb potential. *J. Chem. Phys.* **2003**, *118*, 8207–8215.

(38) Kresse, G.; Hafner, J. Ab initio molecular dynamics for liquid metals. *Phys. Rev. B* **1993**, *47*, 558–561.

(39) Kresse, G.; Furthmüller, J. Efficient iterative schemes for ab initio total-energy calculations using a plane-wave basis set. *Phys. Rev. B* **1996**, *54*, 11169–11186.

(40) Kresse, G.; Joubert, D. From ultrasoft pseudopotentials to the projector augmented-wave method. *Phys. Rev. B* **1999**, *59*, 1758–1775.

(41) Blöchl, P. E. Projector augmented-wave method. *Phys. Rev. B* **1994**, *50*, 17953–17979.

(42) Jepson, O.; Anderson, O. K. The electronic structure of h.c.p. Ytterbium. *Solid State Commun.* **1971**, *9*, 1763–1767.

(43) Lehmann, G.; Taut, M. On the Numerical Calculation of the Density of States and Related Properties. *Phys. Stat. Sol. (b)* **1972**, *54*, 469.

(44) Blöchl, P. E.; Jepsen, O.; Andersen, O. K. Improved tetrahedron method for Brillouin-zone integrations. *Phys. Rev. B* **1994**, *49*, 16223–16233.

(45) Jain, A.; Ong, S. P.; Hautier, G.; Chen, W.; Richards, W. D.; Dacek, S.; Cholia, S.; Gunter, D.; Skinner, D.; Ceder, G. et al. Commentary: The Materials Project: A materials genome approach to accelerating materials innovation. *APL Mater.* **2013**, *1*, 011002.

(46) Sheppard, D.; Terrell, R.; Henkelman, G. Optimization methods for finding minimum energy paths. *J. Chem. Phys.* **2008**, *128*, 134106.

(47) Euchner, H.; Groß, A. Atomistic modeling of Li- and post-Li-ion batteries. *Phys. Rev. Materials* **2022**, *6*, 040302.

(48) Vidal-Valat, G.; Vidal, J.-P.; Zeyen, C. M.; Kurki-Suonio, K. Neutron diffraction study of magnesium fluoride single crystals. *Acta Cryst. B* **1979**, *35*, 1584–1590.

(49) Roessler, D. M.; Walker, W. C. Electronic Spectrum and Ultraviolet Optical Properties of Crystalline MgO. *Phys. Rev.* **1967**, *159*, 733–738.

(50) Helmbrecht, K.; Euchner, H.; Groß, A. Revisiting the Chevrel Phase: Impact of Dispersion Corrections on the Properties of Mo6S8 for Cathode Applications**. *Batteries Supercaps* **2022**, e202200002.

(51) Song, Z.; Liu, Q. Tolerance Factor and Phase Stability of the Normal Spinel Structure. *Cryst. Growth Des.* **2020**, *20*, 2014–2018.

(52) Sun, W.; Dacek, S. T.; Ong, S. P.; Hautier, G.; Jain, A.; Richards, W. D.; Gamst, A. C.; Persson, K. A.; Ceder, G. The thermodynamic scale of inorganic crystalline metastability. *Sci. Adv.* **2016**, *2*, e1600225.

(53) Dillenz, M.; Sotoudeh, M.; Glaser, C.; Janek, J.; Groß, A.; Euchner, H. Unravelling Charge Carrier Mobility in d0-Metal-based Spinels. *Batteries Supercaps* **2022**, *5*, e202200164.

(54) Bachman, J. C.; Muy, S.; Grimaud, A.; Chang, H.-H.; Pour, N.; Lux, S. F.; Paschos, O.; Maglia, F.; Lupart, S.; Lamp, P. et al. Inorganic Solid-State Electrolytes for Lithium Batteries: Mechanisms and Properties Governing Ion Conduction. *Chem. Rev.* **2016**, *116*, 140–162.